Supporting Information for

Intense Ultraviolet Upconversion Emissions in Water-Dispersed Colloidal $YF_3:Yb^{3+}/Tm^{3+}$ Rhombic Nanodisks

Hailong Qiu,[adf] Guanying Chen*[af], Rongwei Fan,[b] Liming Yang,[c] Cheng Liu,[c] Shuwei Hao,[a] Michael J. Sailor,[d] Hans Ågren,[e] Chunhui Yang*[a] and Paras N. Prasad*[f]

[a]*School of Chemical Engineering and Technology, Harbin Institute of Technology, 150001 Harbin, People's Republic of China. E-mails: guanying@buffalo.edu, yangchh@hit.edu.cn*

[b]*National Key Laboratory of Tunable Lasers, Institute of Optical Electronics, Harbin Institute of Technology, 150001 Harbin, People's Republic of China*

[c]*Department of Pathophysiology, Harbin Medical University, 150001 Harbin, People's Republic of China*

[d]*Department of Chemistry and Biochemistry, The University of California, San Diego, 9500 Gilman Drive, La Jolla, California 92093-0358, United States*

[e]*Department of Theoretical Chemistry, Royal Institute of Technology, S-10691 Stockholm, Sweden*

[f]*Institute for Lasers, Photonics, and Biophotonics, The State University of New York at Buffalo, Buffalo, New York 14260, United States. E-mail: pnprasad@buffalo.edu.*

[g]Department of Chemistry, Korea University, Seoul 136-701, Korea

Materials

All reagents were of analytical grade and used without further purification. Y_2O_3, Yb_2O_3, and Tm_2O_3 (purity ≥ 99.99 %) were supplied by Beijing Founde Star Science and Technology Co., Ltd China. Oleic acid (OA, 90%) and octadecene (ODE, 90%) of technical grade were obtained from Sigma-Aldrich. Poly(acrylic acid) (PAA) (Mw=1800) and diethylene glycol (DEG) were purchased from Sigma-Aldrich. Ethanol, chloroform, cyclohexane, sodium hydroxide, perchloric acid, nitric acid**,** and trifluoroacetic acid (99%) were supplied by Tianjin Chemical Reagent Company. Deionized water was used throughout the synthesis procedure.

Synthesis of YF_3:Yb^{3+}/Tm^{3+} Rhombic Nanodisks. YF_3:Yb^{3+}/Tm^{3+} rhombic nanodisks codoped with 2 mol% Tm^{3+} and 10, 30, 50, 70, 90 and 98 mol% Yb^{3+} were synthesized using a thermolysis method adapted from our recent work. In a typical procedure, 1 mmol lanthanide oxides (Tm_2O_3, Yb_2O_3, and Y_2O_3) were dissolved in 50% concentrated trifluoroacetic acid at 95 °C in a three-necked 100 mL flask. The molar ratios of the cationic ions of precursors were [Tm/(Tm+Yb+Y)] =0.02, and [Yb/(Tm+Yb+Y)]=0.10, 0.30, 0.50, 0.70, 0.90 and 0.98, for nanodisks of YF_3 doped with 2 mol% Tm^{3+} and 10, 30, 50, 70, 90 and 98 mol% Yb^{3+}, respectively. Then, the solutions were evaporated to dryness under N_2 gas purge. Next, 10 mL of OA and 10 mL ODE were added into the three-necked flask. The resulting solution was heated at 140 °C for 45 min, and then to 320 °C at a rate of about 18 °C/min. The reaction was kept at this temperature for about 1 h per min under N_2 gas protection. A needle was used to let the N_2 gas out during the synthesis. After cooling down to room temperature, the resulting products were precipitated by ethanol and collected by centrifugation at 5000 rpm for 5 min. The precipitate was then purified with ethanol three times, and finally dispersed in cyclohexane or chloroform for further uses.

Ligand Exchange of the Oleic Acid with the Polyacrylic Acid. The ligand exchange procedure is adapted from a literature work.[S1,S2] In a typical procedure, a mixture of

DEG (8.0 mL) and PAA (0.1 g) was heated to 110 °C with vigorous stirring under N_2 flow. Then, 2 mL chloroform solution of YF_3:Yb^{3+}/Tm^{3+} rhombic nanodisks (50 mg/mL) were injected and the system was heated to 240 °C for 5 min. During this process, the initial milky solution gradually became clear. After cooling to room temperature, an excess of diluted hydrochloric aqueous solution was added in into the solution until a white precipitation is seen. The precipitation was collected by centrifugation, washed three times with pure water, and neutralized with a diluted solution of sodium hydroxide. Finally, the YF_3:Yb^{3+}/Tm^{3+} nanodisks are dispersed in deionized water.

Characterization

X-ray Diffraction. The powder X-Ray diffraction (XRD) pattern was carried out on a Rigaku D/max-γB diffractometer equipped with a rotating anode and a Cu Kα source (λ=0.15418 nm). The 2θ angle of the XRD spectra was recorded at a scanning rate of 5 °/min from 20° to 90°.

Transmission Electron Microscopy. The morphology and size of the resulting nanoparticles were investigated by means of transmission electron microscope (TEM, Tecnai G2 Spirit Twin 12) operating at 80 kV. High resolution transmission electron microscopic (HRTEM) images were obtained on the microscope of Spirit Twin Tecnai G2 D339 operating at 300 kV. One drop of diluted colloidal YF_3 solution dispersed in cyclohexane or water was allowed to be dried on the surface of the carbon-coated copper grid.

Fourier Transform Infrared Spectra. Fourier transform infrared (FT-IR) spectra were measured on an IRPRESTIGE-21 spectrometer utilizing the potassium bromide (KBr) pellet technique. To make the KBr pelletes, 1 mg of YF_3 nanoparticles were mixed with approximately 100 mg KBr powder. The FT-IR spectrum was collected in the spectral range of 400-4000 cm^{-1}.

Upconversion Spectra. Upconversion spectra UC PL spectra were recorded using a lens-coupled monochromator (Zolix Instruments Co. Ltd., Beijing) with a slit width defining spectral resolution of 2 nm. The emissions were excited at 980 nm using a fiber-coupled laser diode (Hi-Tech Optoelectronics Co. Ltd., Beijing). All measurements were performed at room temperature, preserving the same geometry for the upconversion luminescence recording. Photographic images of colloidal nanocrystals YF_3:Yb^{3+}/Tm^{3+} were taken by a digital camera (Canon Power Shot SX100 IS) without adding any filter.

Inductively Coupled Plasma Atomic Emission Spectra. The composition of the resulting nanoparticles was determined by an inductively coupled plasma atomic emission spectroscopy (ICP-AES) (VistaPro, Varian). The samples (200 μL, 5mg/mL) were firstly dissolved in concentrated perchloric acid (2 mL) at 80 °C for 6 h. Then, the solutions were diluted with 1% HNO_3 to a volume of 10 mL.

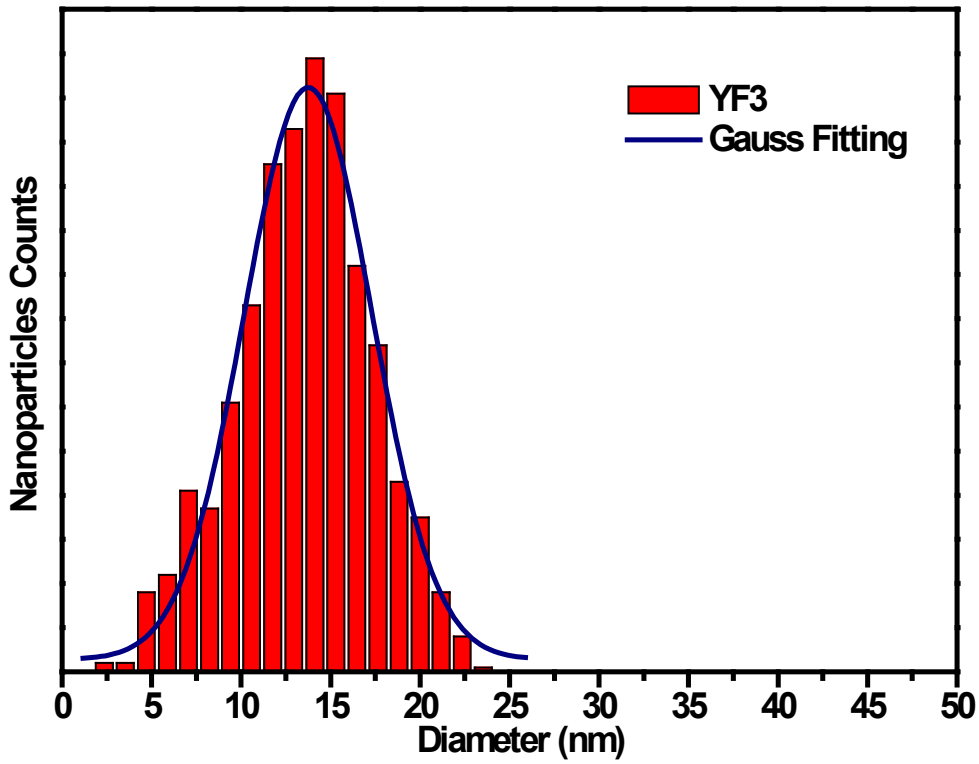

Figure S1. Histogram of the side length of rhombic nanodisks of YF_3 codoped with 10 mol% Yb^{3+} and 2 mol% Tm^{3+}. These data were obtained from the TEM images of more than 200 nanoparticles. The average side length of rhombic nanodisks was determined be ~14.3 nm with a standard deviation of 1.0 nm.

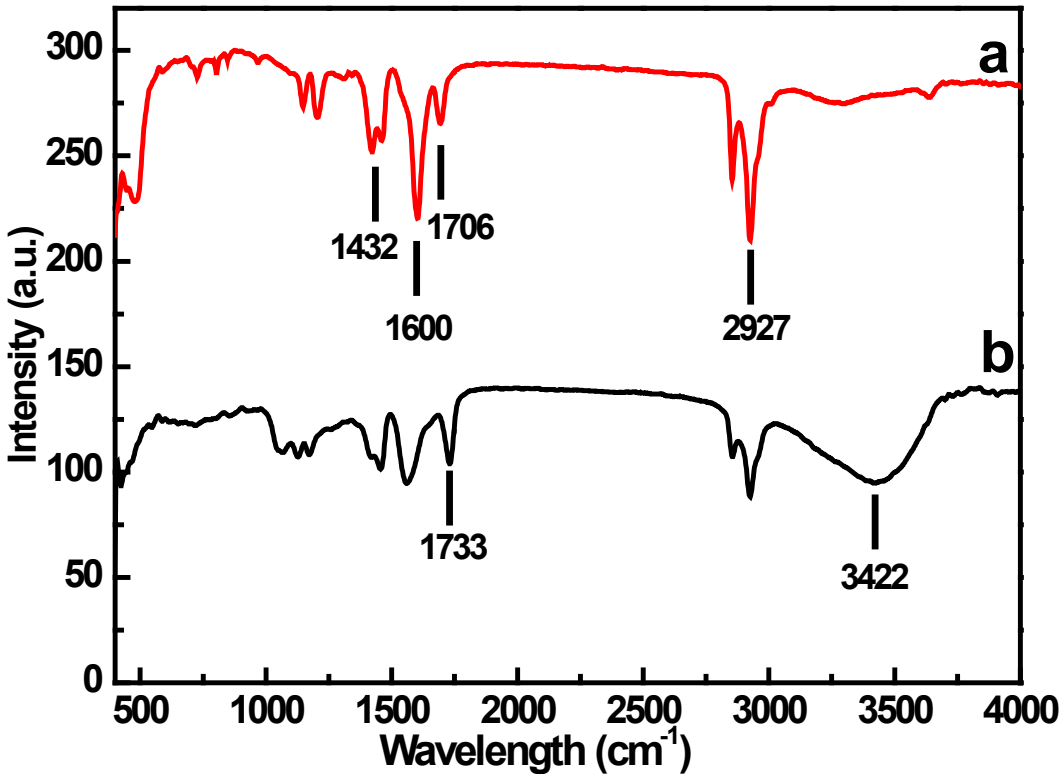

Figure S2. Fourier transform infrared (FTIR) spectra of YF_3 rhombic nanodisks before (a) and after (b) ligand exchange with ployacrylic acid (PAA). The bands at 1432 and 1600 cm^{-1} in Figure S2(a) arise from the ansymmetric and symmetric vibration modes of the -COOH group, respectively, indicating the adsorption of OA on the nanodisk surface through a bidentate bond. The intensities of these two bands become weaker after ligand exchange in Figure S2 (b). The weak stretching mode of the -COOH group at 1706 cm^{-1} in Figure S2(a) suggests the presence of trace amount of free oleic acid on the surface of rhombic nanodisk. However, this band is enhanced and shifted to 1732 cm^{-1} after ligand exchange with PAA (Figure S2 (b)), suggesting an increase in the number of -COOH groups. Additionally, the shoulder at 2927 cm^{-1}, associated with the asymmetrical stretching mode of $-CH_3$ group, became weaker after ligand exchange, showing that the number of the $-CH_3$ groups is reduced on the nanodisk surface after ligand exhange. The broad band at 3100-3600 cm^{-1} arises from the O-H stretching vibration of -COOH group in Figure S2 (a), which becomes much stronger in Figure S2 (b). Since the PAA ligands have abundant COOH groups, the increased number of COOH group confirms that PAA have been introduced onto the nanodisk surface. These observations give a strong evidence of the successful exchange of OA with PAA.

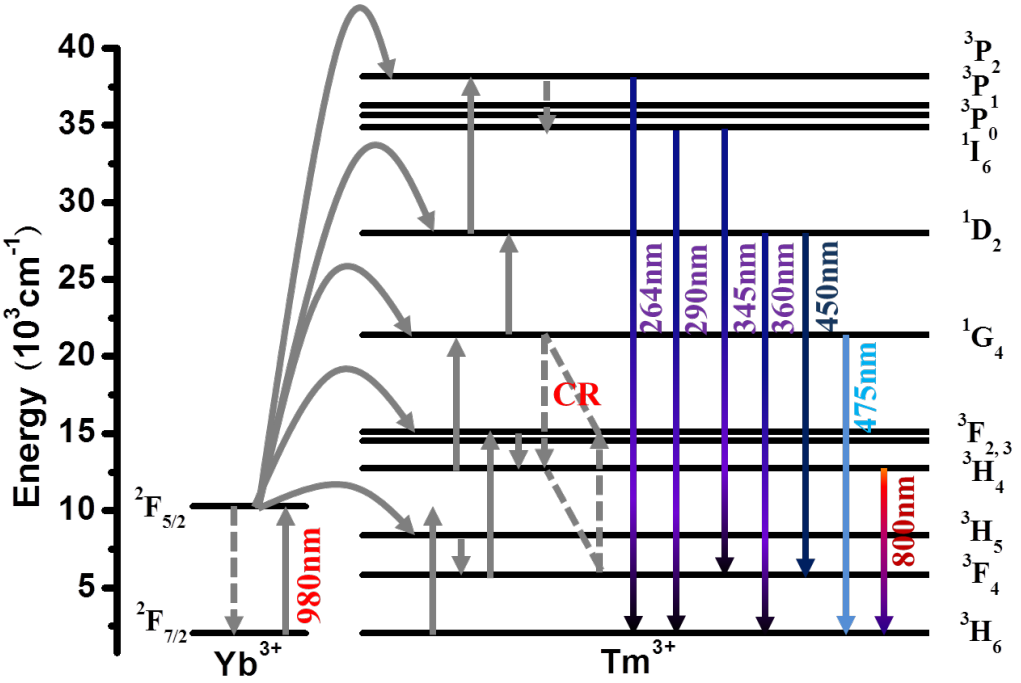

Figure S3. Energy level diagrams of Yb^{3+} and Tm^{3+} ions as well as the proposed upconversion mechanisms for different emission bands (λex= 980 nm). The Yb^{3+} ions firstly absorbs laser photons at ~980 nm, and are excited from the ground state $^2F_{5/2}$ to the $^2F_{7/2}$ state. Then, the Yb^{3+} ions in their excited states successively transfer the absorbed energy to the Tm^{3+} ion, and promote it from the ground sate to the $^3H_5$ (first step), $^3F_{2,3}$ (second step), $^1G_4$(third step), $^1D_2$(fourth step), and $^3P_1$(fifth step) states, respectively. Multi-phonons from the lattice are involved to assist the energy transfer from Yb^{3+} to Tm^{3+} ions. Nonradiative relaxations from the $^3F_{2,3}$ state can populate the $^3H_4$ state, from which the near infrared (NIR) emission at 800 is produced. It should be noted that the cross-relaxation process of $^1G_4+{}^3F_4 \rightarrow {}^3H_4+{}^3F_2$ can contribute to populate the $^3H_4$ state, thus might leading to slightly larger photon process than 2 for NIR emission at 800 nm. In addition, nonradiative relaxations from the $^3P_1$ state can populate the $^1I_6$ state, from which ultraviolet (UV) emission at 290 and 345 nm can be generated by radiative relaxations to the ground state $^3H_6$ and the first excited state of $^3F_4$, respectively. The upconversion emissions at 360 and 450 nm arise from radiative relaxations from the $^1D_2$ state to the ground $^3H_6$ and the excited state of $^3F_4$ of Tm^{3+} ions, respectively. The blue emission at 475 nm stems from radiative relaxations from the $^1G_4$ state to the ground $^3H_6$ state.

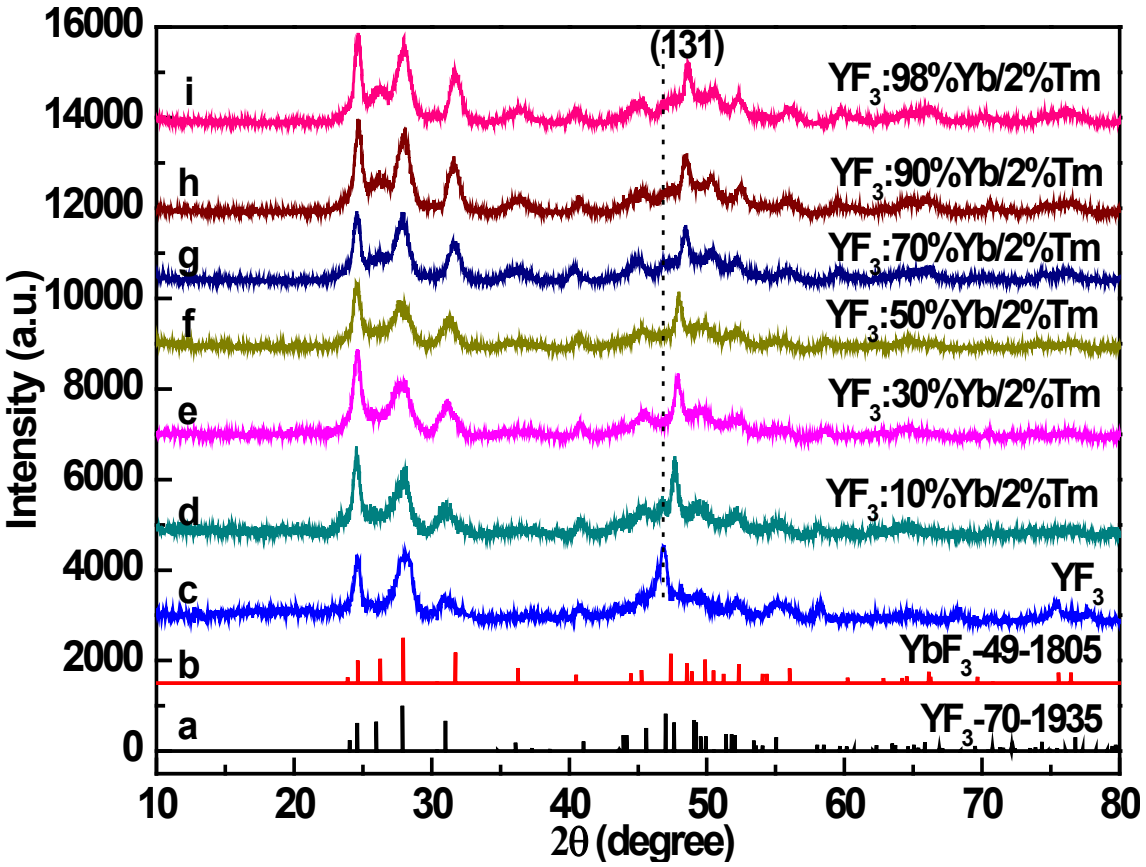

Figure S4. XRD patterns of (a) standard data of orthorhombic YF_3 (JCPDS Card No. 70-1935), (b) standard data of orthorhombic YbF_3 (JCPDS Card No. 49-1805), as well as rhobmbic nanodisks of (c) pure YF_3 (without doping), (d) YF_3:10 mol%Yb^{3+}/2 mol%Tm^{3+} (e) YF_3:30 mol%Yb^{3+}/2 mol%Tm^{3+}, (f) YF_3:50 mol%Yb^{3+}/2 mol%Tm^{3+} (g) YF_3: mol%Yb^{3+}/2 mol%Tm^{3+} (h) YF_3:90 mol%Yb^{3+}/2 mol%Tm^{3+}, and (i) YF_3:98 mol%Yb^{3+}/2 mol%Tm^{3+}.

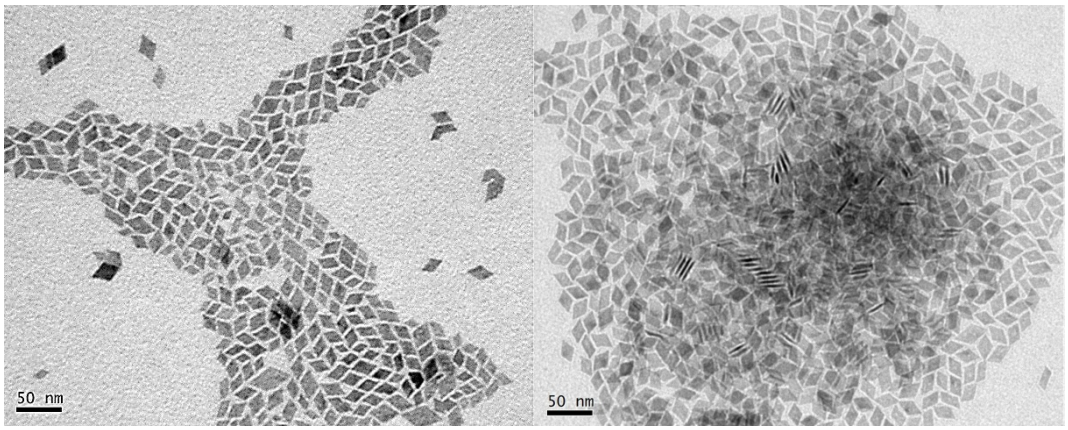

Figure S5. TEM images of rhobmbic nanodisks of YF_3:10 mol%Yb^{3+}/2 mol%Tm^{3+} (left) before and (right) after ligand exchange.

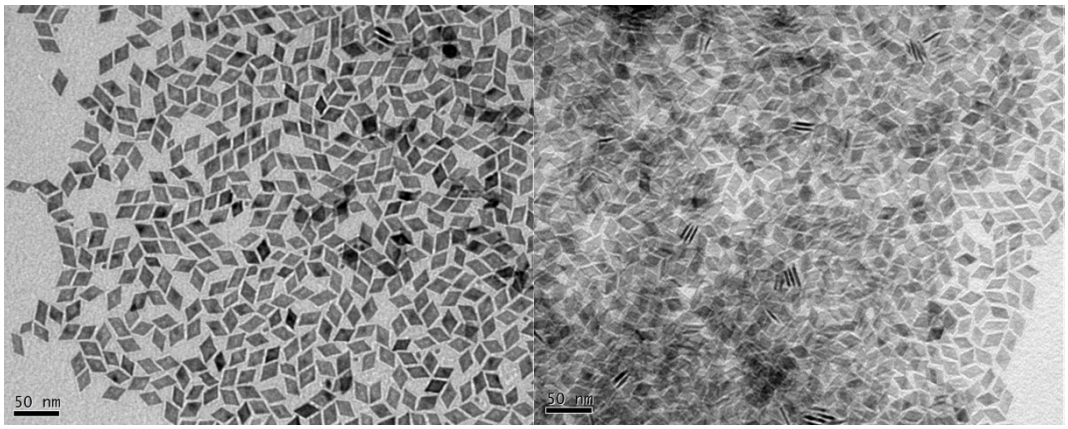

Figure S6. TEM images of rhobmbic nanodisks of YF_3:30 mol%Yb^{3+}/2 mol%Tm^{3+} (left) before and (right) after ligand exchange.

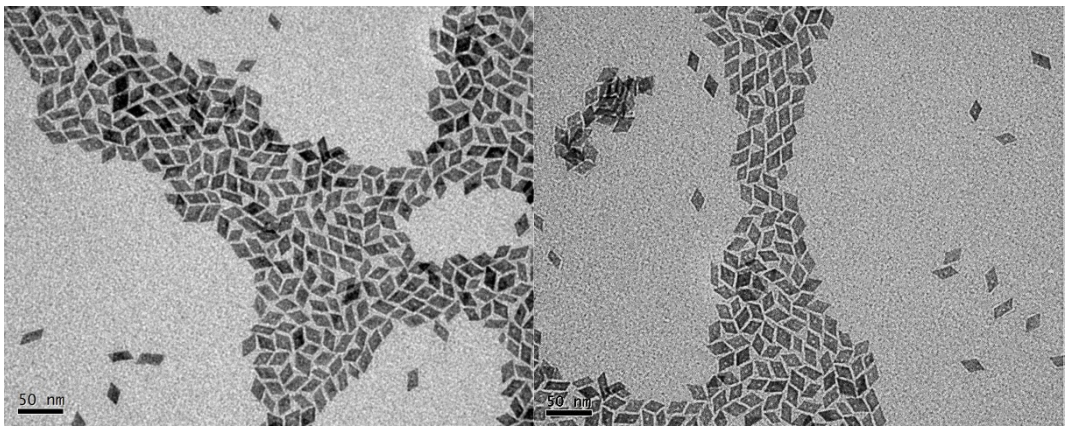

Figure S7. TEM images of rhobmbic nanodisks of YF_3:50 mol%Yb^{3+}/2 mol%Tm^{3+}

(left) before and (right) after ligand exchange.

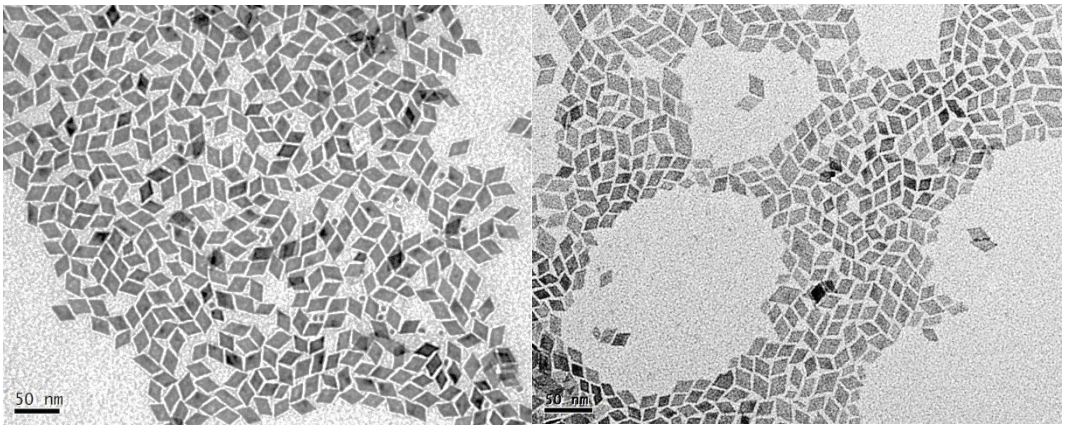

Figure S8. . TEM images of rhobmbic nanodisks of YF_3:70 mol%Yb^{3+}/2 mol%Tm^{3+} (left) before and (right) after ligand exchange.

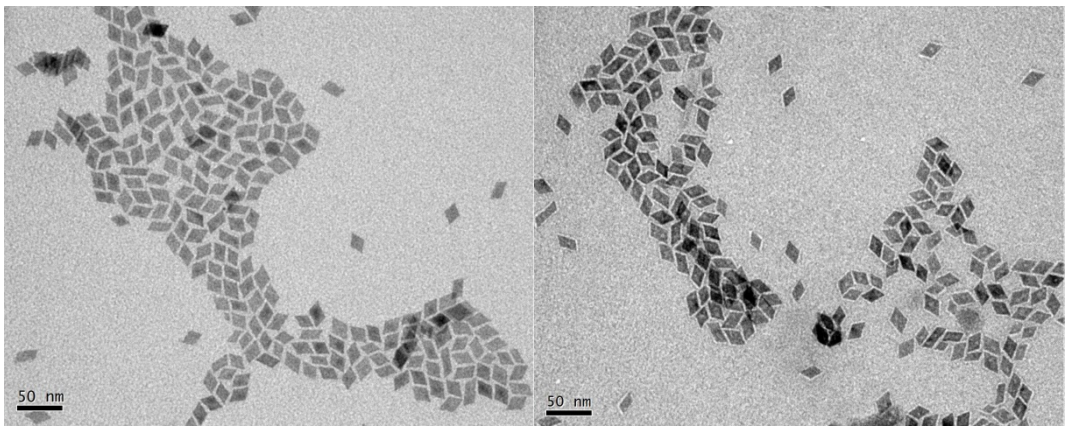

Figure S9. . TEM images of rhobmbic nanodisks of YF_3:90 mol%Yb^{3+}/2 mol%Tm^{3+} (left) before and (right) after ligand exchange.

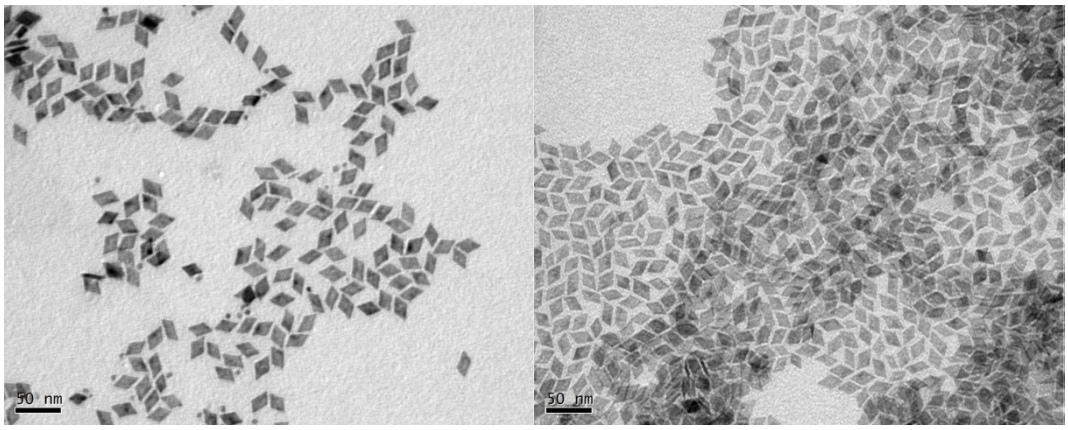

Figure S10. . TEM images of rhobmbic nanodisks of YbF_3: 2 mol%Tm^{3+} (left) before and (right) after ligand exchange.

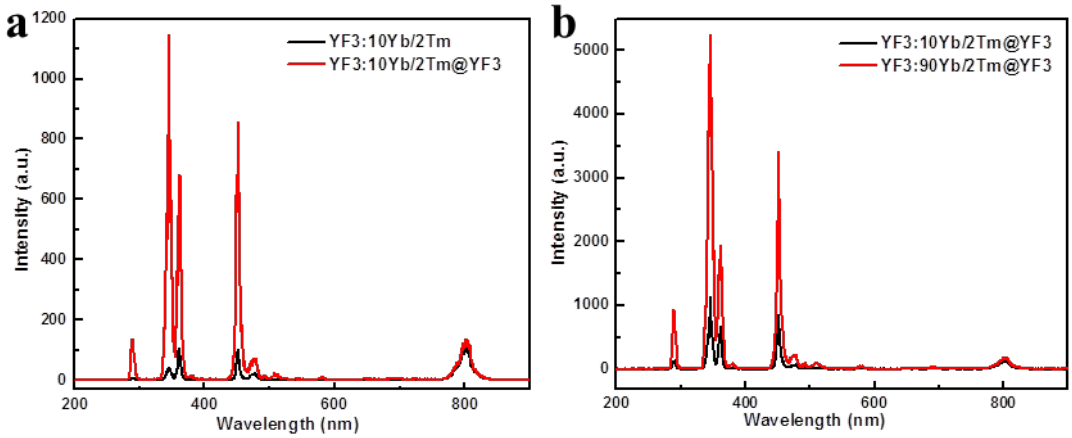

Figure S11. Room temperature upconversion emission spectra of (a) YF_3: 10 mol%Yb^{3+}/2 mol%Tm^{3+} core and YF_3: 10 mol%Yb^{3+}/2 mol %Tm^{3+}@YF_3 core/shell nanoparticles, and (b) YF_3: 10 mol %Yb^{3+}/2 mol%Tm^{3+}@YF_3 and YF_3: 90 mol %Yb^{3+}/2 mol%Tm^{3+}@YF_3 core/shell nanoparticles.

The increase of Yb^{3+} ions can produce two distinct effects on the upconversion emissions. (i) Enhancing upconversion emission intensities due to elevated energy transfers from Yb^{3+} to Tm^{3+} ions; (ii) Quenching upconversion emission intensities due to Yb^{3+} sublattice-mediated energy transfer of excitation energy to nanoparticle

surface quenching centers. The quenching mechanism, however, can be eliminated or effectively suppressed by growing an inert shell layer on the particle surface. Hence, to confirm our proposed enhancement mechanism for Fig.4, we have prepared core/shell structure nanoparticles of YF_3:10 mol %Yb^{3+}/2 mol %Tm^{3+}@YF_3 and YF_3: 90 mol%Yb^{3+}/2 mol%Tm^{3+}@YF_3, wherein the quenching mechanism induced by Yb^{3+} ion has been suppressed. Figure S11 displays upconversion emission spectra of (a) YF_3: 10 mol%Yb^{3+}/2 mol%Tm^{3+} core and YF_3: 10 mol%Yb^{3+}/2 mol%Tm^{3+}@YF_3 core/shell nanoparticles, as well as (b) YF_3:10 mol%Yb^{3+}/2 mol%Tm^{3+}@YF_3 and YF_3:90 mol%Yb^{3+}/2 mol%Tm^{3+}@YF_3 core/shell nanoparticles. In comparison to the emission intensity of core nanoparticles of YF_3: 10 mol%Yb^{3+}/2 mol%Tm^{3+}, the emission intensity in the YF_3: 10 mol%Yb^{3+}/2 mol%Tm^{3+}@YF_3 core/shell nanoparticles is significantly increased, indicating the successful growth of an YF_3 layer on the surface of core nanoparticles [Figure S11 (a)]. Moreover, in Figure S11 (b), it is shown that UV upconversion emission in YF_3:90 mol%Yb^{3+}/2 mol%Tm^{3+}@YF_3 core/shell nanoparticles is about 5 times higher than that of the YF_3:10 mol%Yb^{3+}/2 mol%Tm^{3+}@YF_3 nanoparticles, clearly substantiating our proposed mechanism in this work.

Table S1. Compositions of these nanodisks of YF_3 codoped with 2 mol% Tm^{3+} and 10-98 mol% Yb^{3+}. These compostions are determined by inductively coupled plasma atomic emission spectroscopy (ICP-AES). The measured atomic ratios are in good agreement with the ratios of precursors that are employed for nanoparticle synthesis.

Sample	**The mole ration of doped [Ln^{3+}] in NCs (at. %) [Y^{3+}] : [Yb^{3+}] : [Tm^{3+}]**
YF_3:10%Yb^{3+}/2%Tm^{3+}	86.45 : 11.43 : 2.12
YF_3:30%Yb^{3+}/2%Tm^{3+}	67.30 : 29.89 : 2.81
YF_3:50%Yb^{3+}/2%Tm^{3+}	48.23 : 50.07 : 1.70
YF_3:70%Yb^{3+}/2%Tm^{3+}	28.93 : 69.09 : 1.98
YF_3:90%Yb^{3+}/2%Tm^{3+}	08.63 : 89.26 : 2.11
YF_3:98%Yb^{3+}/2%Tm^{3+}	00.00 : 97.32 : 2.68

Reference:

S1. T. Zhang, J. Ge, Y. Hu and Y. D. Yin, *Nano Lett.*, 2007, **7**, 3203.

S2. H. L. Qiu, G. Y. Chen, L. Sun, G. Han, C. H. Yang, *J. Mater. Chem.*, 2011, **21**, 17202.